

Dynamic behavior of frozen soil under uniaxial strain and stress conditions*

Hai-dong ZHANG (张海东)¹, Zhi-wu ZHU (朱志武)^{1,2},
Shun-cheng SONG (宋顺成)¹, Guo-zheng KANG (康国政)¹,
Jian-guo NING (宁建国)³

- (1. Traction Power State Key Laboratory, Southwest Jiaotong University,
Chengdu 610031, P. R. China;
2. State Key Laboratory of Frozen Soil Engineering, Cold and Arid Regions Environmental and
Engineering Research Institute, Chinese Academic Sciences, Lanzhou 730000, P. R. China;
3. State Key Laboratory of Explosion Science and Technology,
Beijing Institute of Technology, Beijing 100081, P. R. China)

Abstract The split Hopkinson pressure bar (SHPB) method is used to investigate the dynamic behavior of the artificial frozen soil under the nearly uniaxial strain and uniaxial stress conditions. The tests are conducted at the temperatures of -3°C , -8°C , -13°C , -17°C , -23°C , and -28°C and with the strain rates from 900 s^{-1} to 1500 s^{-1} . The nearly uniaxial stress-strain curves exhibit an elastic-plastic behavior, whereas the uniaxial stress-strain curves show a brittle behavior. The compressive strength of the frozen soil exhibits the positive strain rate and negative temperature sensitivity, and the final strain of the frozen soil shows the positive strain rate sensitivity. The strength of the frozen soil under the nearly uniaxial strain is greater than that under the uniaxial stress. After the negative confinement tests, the specimens are compressed, and the visible cracks are not observed. However, the specimens are catastrophically damaged after the uniaxial SHPB tests. A phenomenological model with the thermal sensitivity is established to describe the dynamic behavior of the confined frozen soil.

Key words frozen soil, dynamic loading, split Hopkinson pressure bar (SHPB), confinement, high strain rate

Chinese Library Classification O347, P642

2010 Mathematics Subject Classification 74L10, 76L05

1 Introduction

The 23% vast regions of the world's land surface at the mid-to-high latitudes and the high altitudes are covered by perennial frozen soil^[1]. Economic, scientific, and technological developments, which have enabled the ongoing migration of civilization to such cold regions, have

* Received May 23, 2012 / Revised Oct. 30, 2012

Project supported by the National Natural Science Foundation of China (No. 11172251), the Open Fund of State Key Laboratory of Frozen Soil Engineering (No. SKLFSE201001), and the Fundamental Research Funds for the Central Universities (No. SWJTU09CX069)

Corresponding author Zhi-wu ZHU, Associate Professor, Ph.D., E-mail: zzw4455@163.com

stimulated much research in such areas including the study of the mechanical behavior of the frozen soil in depth.

Most current research is focused on the static or quasi-static behavior of the frozen soil^[2–3]. Except for the static and quasi-static loads, the frozen soil is often subjected to the dynamic or high strain rate loads that occur during blasting and excavation, both of which are poorly studied. Therefore, the dynamic behavior of the frozen soil needs to be studied and furthermore the dynamic constitutive models need to be established.

The split Hopkinson pressure bar (SHPB) method has played a significant role in the dynamic testing of materials. Even though it was originally developed for metals, it has been widely applied to geomaterials such as rocks and concretes. Soft geomaterials like sand and clay were also tested by a modified SHPB technique^[4–5], which implied that it was also possible to use this method for the frozen soil. The Sandia National Laboratory in the USA carried out the SHPB tests under the negative lateral confinement or nearly uniaxial strain conditions on the artificial frozen soils modeled on the Alaskan examples^[6]. Recently, they conducted more SHPB tests on the undisturbed frozen soil from Alaska and attempted to describe its constitutive behavior using a cap plasticity model^[7]. However, due to the complexity and heterogeneity of the undisturbed frozen soil, their later test results dispersed sharply, and the model could not adequately describe the dynamic behavior. Ma^[8] studied the dynamic behavior of the artificial frozen soil consisting of clay from a coal mine, which showed the dependence on both the temperature and the strain rate. However, this result, which suggests the convergence of the stress-strain profiles with the same temperature but different strain rates, seems to be counterintuitive compared with other geomaterials.

To better understand the high strain rate behavior of the frozen soil, two series of SHPB tests, one under the nearly uniaxial strain conditions and the other under the uniaxial stress conditions, were undertaken at Southwest Jiaotong University, Chengdu. The effects of the strain rate, the temperature, and the stress state are investigated.

2 Experimental procedures

2.1 Material and specimens

The material studied here is the frozen Chengdu clay. All the specimens in this study have a moisture content of about 20% by weight and a dry density of approximately 1.6 g/cm^3 . Due to the heterogeneity of the frozen soil, the specimens must be sufficiently large. The dimensions of all the specimens for the tests are $\Phi 30 \text{ mm} \times 18 \text{ mm}$.

The soil sample used here is extracted from a railway construction site in Chengdu, Sichuan Province. The undisturbed sample is first crushed down with a wooden hammer. The large grains are then sifted out of the sample using a sieve with a mesh size of 2 mm. The sifted material is then placed in a dry electric oven at a preset temperature of 105°C for 12 h to be dehydrated. By sifting 300 g of the dried soil sample with four sieves in succession, of which the hole diameters are 2 mm, 0.5 mm, 0.25 mm, and 0.1 mm, and a particle size distribution is obtained (see Table 1). To produce a soil sample with the 20% water content, an appropriate amount of distilled water is added into the dried soil sample and mixed uniformly. Then, it is stored in a closed container for 6 h.

Table 1 Particle size distribution

Size/mm	< 0.1	0.1–0.25	0.25–0.5	0.5–2	> 2
Proportion/%	20.78	20.25	0.70	57.16	1.11

The specimens for the tests are incised from the thick specimens so as to make the surface smoother. The uniformly mixed sample with a mass of 64.13 g is placed in a container with an inner diameter of 45 mm and an inner height of 21 mm. After flattening the upper surface

of the sample, the container is sealed with an imbedded cap. This ultimately results in a $\Phi 45 \text{ mm} \times 21 \text{ mm}$ thick specimen. The thick specimen is then cut with the assistance of a cutting ring, which is 18 mm in the height and 30 mm in the inner diameter. The sample is then smoothed to produce a $\Phi 30 \text{ mm} \times 18 \text{ mm}$ specimen. A thin layer of the petroleum jelly must be smeared on the surface of the specimen to prevent the evaporation of water. Now, the well-made specimen is placed in a refrigerator at the desired temperature for 24 h.

2.2 Dynamic experiments

The SHPB is used to investigate the dynamic compressive behavior of the frozen soil under the uniaxial stress and nearly uniaxial strain conditions. The striker is made of 35CrMnSi steel with the density $\rho = 7900 \text{ kg/m}^3$ and Young's modulus $E = 210 \text{ GPa}$. It has a diameter of 14.5 mm and a length of 200 mm. A conic variable cross-sectional part is placed at the impact end of the incident bar to match the dimensions of the specimens. The length of the $\Phi 14.5 \text{ mm}$ part is 5 mm, the length of the variable section part is 20 mm, and the length of the $\Phi 30 \text{ mm}$ part is 500 mm, running from the impact end to the specimen end of the incident bar. The transmission bar has a length of 400 mm and a diameter of 30 mm. Due to the low strength of the frozen soil, 7075-T6 aluminum is chosen to manufacture the incident and transmission bars. The aluminum has a density of 2810 kg/m^3 and Young's modulus of 71 GPa. The strain gauges connected to an oscilloscope are mounted on the central surface of the incident and transmission bars to capture the incident signal ε_i , the reflected signal ε_r , and the transmitted signal ε_t .

Based on the one-dimensional stress wave theory^[9], the strain rate, strain, and stress history of the specimen can be calculated from the above three signals using the following equations:

$$\begin{cases} \dot{\varepsilon}(t) = \frac{v_1 - v_2}{l_s} = \frac{C_0}{l_s}(\varepsilon_i - \varepsilon_r - \varepsilon_t), \\ \varepsilon(t) = \frac{C_0}{l_s} \int_0^t (\varepsilon_i - \varepsilon_r - \varepsilon_t) dt, \\ \sigma(t) = \frac{1}{2} \left(\frac{A}{A_s} E (\varepsilon_i + \varepsilon_r) + \frac{A}{A_s} E \varepsilon_t \right) = \frac{A}{2A_s} E (\varepsilon_i + \varepsilon_r + \varepsilon_t), \end{cases} \quad (1)$$

where l_s is the length of the specimen, A_s and A are the original cross-sectional areas of the specimen and the bars, respectively, E and C_0 are Young's modulus and the elastic wave speed of the bars, respectively, ε_i and ε_r are the axial incident and reflected strains on the incident bar, respectively, and ε_t is the transmitted axial strain on the transmission bar.

By introducing the assumption of the uniform stress, $\varepsilon_i + \varepsilon_r = \varepsilon_t$, Eq. (1) can be simplified as

$$\begin{cases} \dot{\varepsilon}(t) = -\frac{2C_0}{l_s} \varepsilon_r, \\ \varepsilon(t) = -\frac{2C_0}{l_s} \int_0^t \varepsilon_r dt, \\ \sigma(t) = \frac{A}{A_s} E \varepsilon_t. \end{cases} \quad (2)$$

All the strain, stress, and strain rate data presented here are derived from Eq. (2). The typical incident, reflected, and transmitted waves are shown in Fig. 1.

During the tests, the specimens are placed in a suit or jacket (see Fig. 2) made of 45 steel with an inner diameter of 30.5 mm, an outer diameter of 40 mm, and a length of 40 mm, which is used to restrict the radial deformation and provide a nearly uniaxial strain stress state. The suit is cooled together with the specimens before the test.

3 Results

The confined SHPB tests are conducted on the frozen soil at six different temperatures: -3°C , -8°C , -13°C , -17°C , -23°C , and -28°C , and 3 to 4 different high strain rates:

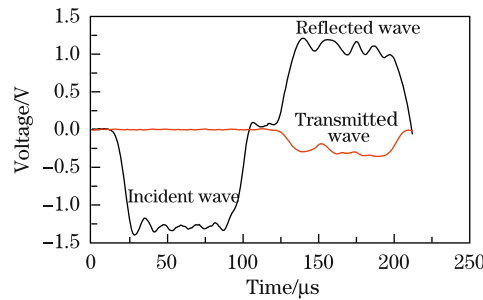


Fig. 1 Typical incident, reflected, and transmitted waves for confined tests

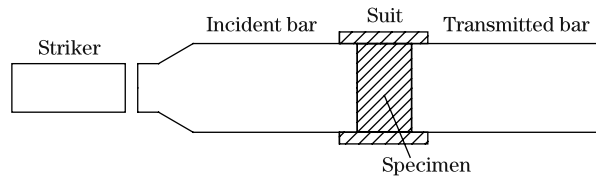


Fig. 2 Schematic diagram of SHPB apparatus with suit

900 s^{-1} to 1500 s^{-1} . The uniaxial stress SHPB tests are conducted on the -3°C and -28°C frozen soil with the strain rate also varying from 900 s^{-1} to 1500 s^{-1} . Because of the existence of the petroleum jelly on the surface of the specimens, the friction between the specimens and the bars can be neglected.

3.1 Nearly uniaxial strain tests

Figure 3 shows the dynamic compressive stress-strain curve of the frozen soil under the confinement at six different temperatures and different strain rates.

In Fig. 3, the stress is observed to rise quickly and nonlinearly at the very beginning, where it reaches the first peak value. Then, the yield stage appears, revealed by a drop in the stress. After the yield, the frozen soil is of nearly perfect plasticity for the low strain rate tests and strain hardening for high strain rate ones until it reaches the peak stress. Then, it is unloaded. Thus, all curves can be divided into four parts^[10]: the nonlinear part before the yield, the yield part, the plastic hardening or the plastic flow portion, and the unloading part. This is consistent with the report in [6]. The first three parts exhibit the uniaxial dynamic compressive stress-strain curves that are very similar to those of the ductile metals. The local peak stress at the yield stage of each curve is defined as the yield strength.

The yield strengths of the frozen soil with the same temperature but at different strain rates are similar. However, the peak stress varies more. Generally, the peak stress increases with the higher loading strain rates. The final strain of each curve behaves in the same manner.

3.2 Uniaxial stress SHPB tests

The stress-strain curves of the uniaxial stress SHPB tests are shown in Fig. 4.

In all cases, the stress gradually drops after the peak stress is observed, and exhibits an elastic brittle behavior. The softening parts of these curves following the peak stress are long, indicating the capacity of the frozen soil after the failure. Although the specimens are broken into dozens of fragments of various sizes during the tests (see the figure (b) in Fig. 5), the load-carrying capacity cannot be neglected.

With the confined experiments, the uniaxial dynamic compressive behavior of the frozen soil is seen to be sensitive to the strain rate and the temperature.

The uniaxial stress-strain curves are very different from the confined ones, indicating a change in the deformation and failure mechanism. Compared with the nearly uniaxial strain or

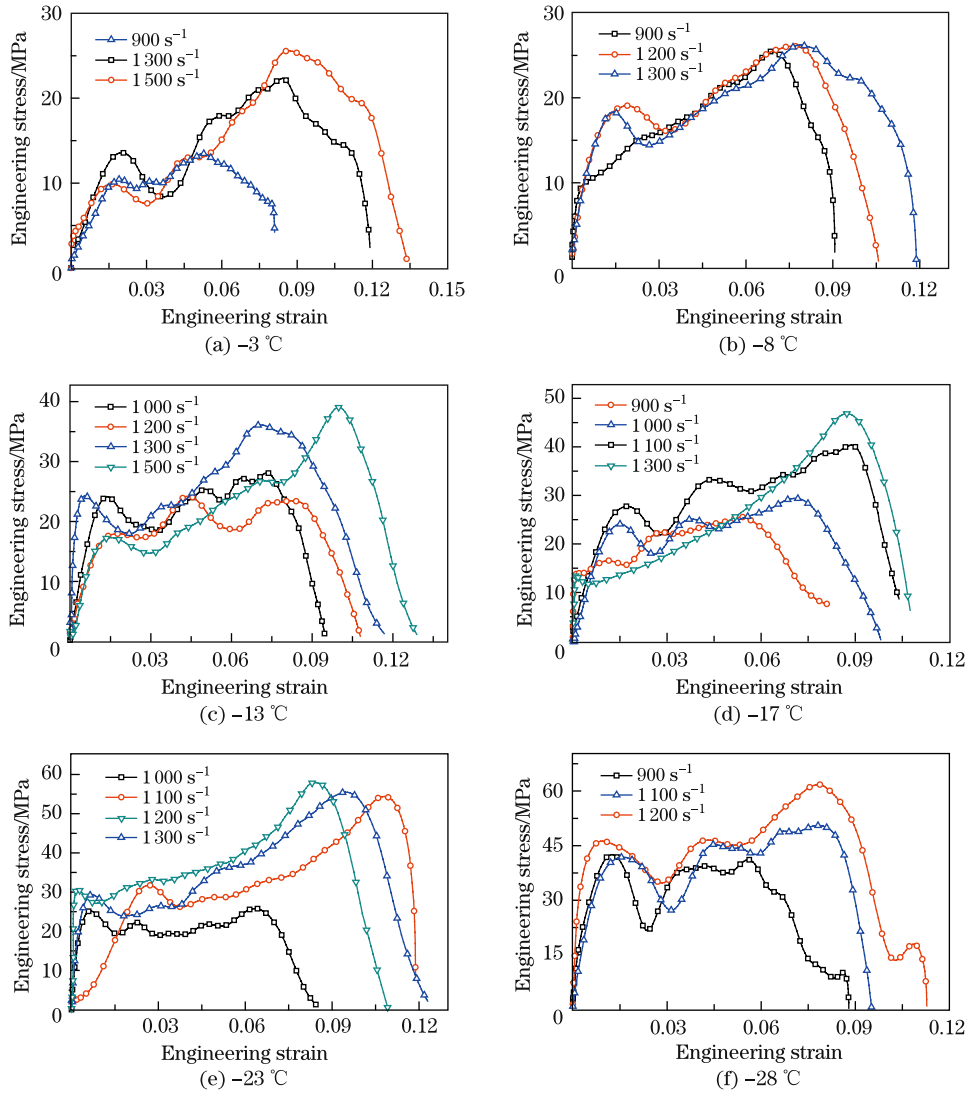


Fig. 3 Stress-strain curves of frozen soil with negative confinement at different strain rates and temperatures

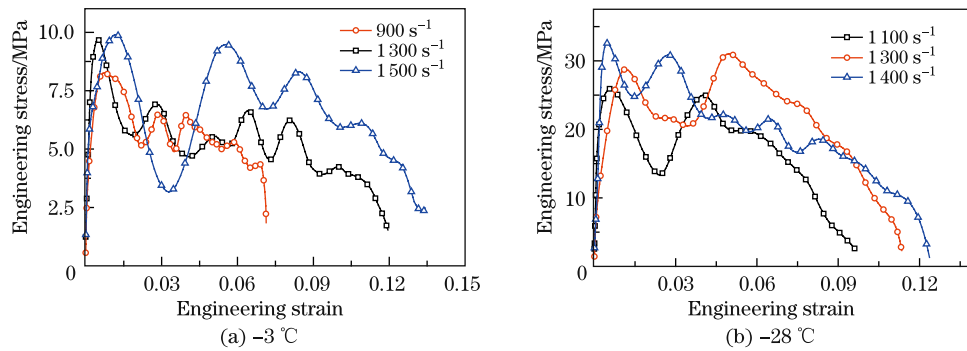


Fig. 4 Uniaxial stress-strain curves of frozen soil of two different temperatures

confined systems, the overall stress levels are lower, and there are no hardening portions in these curves. The peak stress is much lower and almost equal to the yield strength under the confinement with the same conditions. The reason for this phenomenon is the absence of a suit. In the high strain rate uniaxial stress tests, the pores in the frozen soil collapse quickly, and many cracks form and propagate simultaneously and rapidly, causing the failure of the specimens. However, in the nearly uniaxial strain tests, not only is the deformation of the frozen soil restricted, but also the evolution of the damage is modified. The pores are compacted due to the loading and confinement of the suit, even though they start with the collapse at the beginning. Compaction-induced strengthening is greater than damage-induced weakening. The drop in the stress after the initial strength indicates that the damage-induced weakening effect is anterior and more influential than the compaction-induced strengthening effect in the yield stage. These uniaxial curves are totally different from the uniaxial dynamic curves in the report in [7], which may be the result of the frozen soil differences.

4 Discussion

4.1 Deformation of specimens

Because the lateral confinement restricts the evolution of damage in the specimens, they generally appear to remain to be intact without visible cracks after the application of the laterally confined dynamic loads (see Fig. 5(a)). However, the lengths of the specimens are compressed while their diameters are not changed, which implies compaction and consolidation.

In contrast, the specimens subjected to the high strain rate uniaxial tests fail catastrophically, broken into numerous pieces of various dimensions (see Fig. 5(b)).

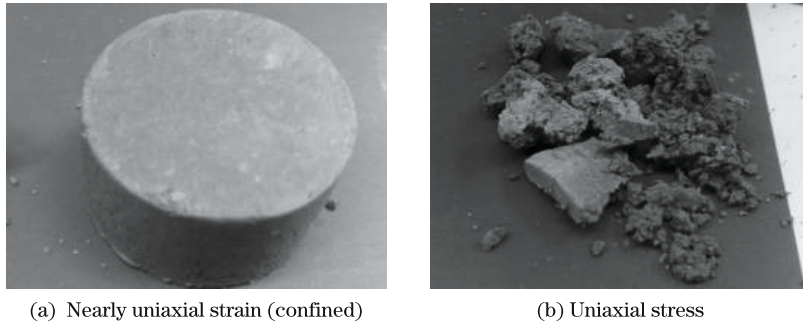


Fig. 5 Frozen soil samples after nearly uniaxial strain and uniaxial stress SHPB tests

Zhu et al.^[11] previously conducted the confined SHPB tests on the soil at the room temperature, showing a different failure mode. In that case, a cylindrical specimen breaks down the middle into two parts due to the tensile wave formed by the reflection of a compressive wave. In the confined tests of the frozen soil, the displacement of the specimen relative to the suit is restricted by the friction between the specimen and the suit resulting from the pressure during the loading process. The compressibility of the frozen soil is much lower than that of the soil at the room temperature, which leads to the higher pressure in the loading process. Moreover, the tensile strength of the frozen soil is higher than that of the soil at the room temperature.

4.2 Strain rate effect

To compare the sensitivity of the strain rate quantitatively, the peak stress and the final strain are plotted against the strain rate data for the confined tests (see Fig. 6). Both the peak stress and the final strain are observed to increase with the increasing strain. In general, the low temperature frozen soil has the higher peak stress. However, the increase of the final strain behaves in an almost linear way with little variation in the case of temperature changes. This result contrasts entirely with the work of Ma^[8].

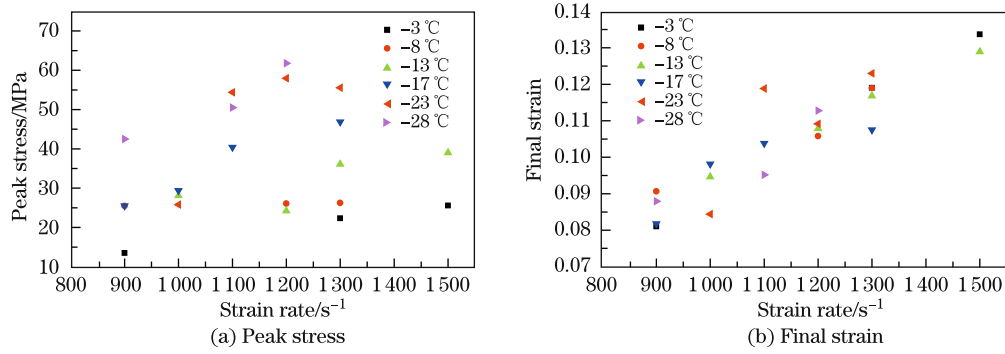


Fig. 6 Peak stress and final strain vs. strain rate relationships for frozen soil at different temperatures under confinement

At the high strain rates, large numbers of cracks in the frozen soil are initialized and developed simultaneously. Furthermore, the number of the cracks that initialize and develop increases with the strain rate, leading to the higher flow stress and the peak stress. The amplitude of the loading stress increases with the higher strain rates under the same conditions. Therefore, the final strain also increases with the higher strain rates.

4.3 Temperature effect

To compare the effect of the frozen soil temperature under the confinement, the stress-strain curves for the same loading rate are shown in Fig. 7.

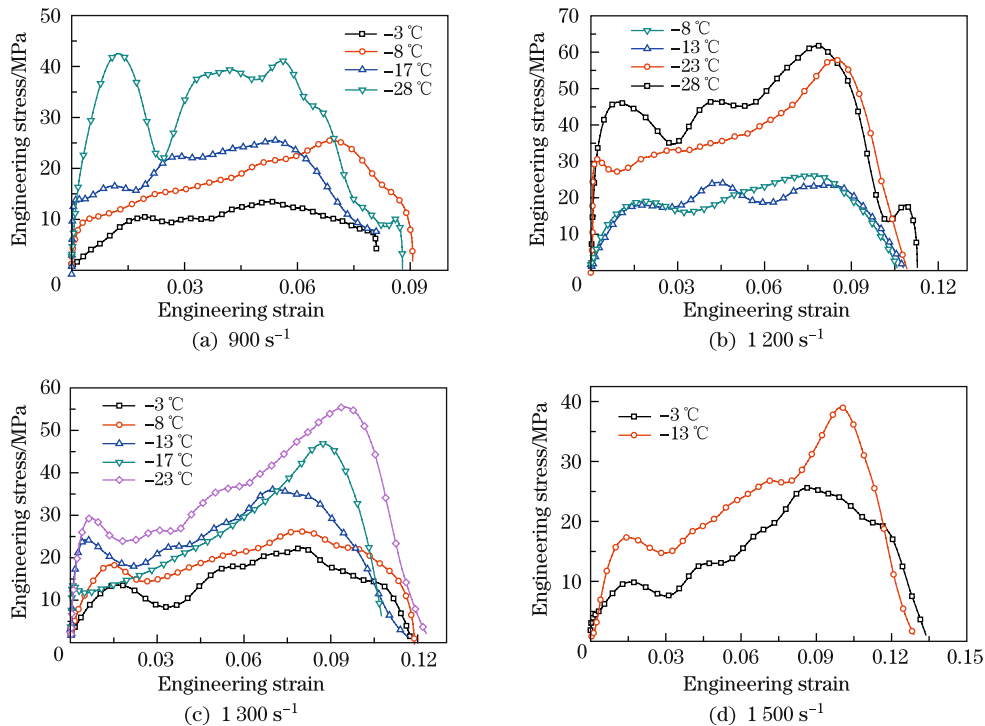


Fig. 7 Stress-strain curves of confined frozen soil at different strain rates and temperatures

It is clear that the dynamic stress-strain curves for different temperatures but with the same strain rate converge or at least have the tendency to converge. This means that the final strains at the same loading strain rate are almost the same.

When the loading strain rate is 900 s^{-1} , the peak stress of the -28°C frozen soil reaches 42.5 MPa. However, it is only 13.3 MPa for the -3°C frozen soil. The peak stress of the -23°C frozen soil is 55.5 MPa, it is 36.1 MPa for the -13°C frozen soil, and it decreases to 22.3 MPa for the -13°C frozen soil with a strain rate of 1300 s^{-1} . Generally, the stress level of the lower temperature frozen soil is higher than that of the higher temperature ones at the same strain rate.

Obviously, the frozen soil behaves with great thermal sensitivity. The frozen soil is composed of ice, mineral grains, unfrozen water, and air. The colder the frozen soil gets, the more the unfrozen water will convert to ice. In addition, the dynamic strength of the ice is higher at the lower temperatures^[12]. Moreover, the cohesive strength between the ice and the mineral particles in the frozen soil becomes higher while the frozen soil cools.

However, for the final strain, it appears that the influence of the temperature with the same strain rate remains to be inconspicuous.

5 Model for confined frozen soil

The significance of the experimental results can be further assessed through the construction of a simple dynamic material model tested by a finite element method (FEM) simulation. Due to the existence of the jacket in the apparatus, it is assumed that the specimen within the jacket undergoes the nearly uniaxial deformation. The changes in temperature during the tests are neglected, and the deformation and failure mechanisms at the meso level are not considered. However, since the frozen soil is thermally sensitive, the temperature should be taken into account. Additionally, the unloading part is not involved in the model. Even though the short yield stages exist in these confined curves, they look very similar to the uniaxial dynamic compressive stress-strain curves of the ductile metals. Assuming that the loading part is elastic, we can neglect the yield stage so that the constitutive behavior of the frozen soil can be described in an elastic-plastic way^[13].

A two-sectional experiential function describing the dynamic stress-strain curves is introduced^[14] as follows:

$$\sigma = \begin{cases} E\varepsilon, & \sigma \leq Y_d, \\ Y\left(\frac{E\varepsilon}{Y_d}\right)^n + \alpha\left(\frac{\dot{\varepsilon}}{\dot{\varepsilon}_0}\right)^m, & \sigma > Y_d, \end{cases} \quad (3)$$

where σ is the stress, ε is the engineering strain, and $\dot{\varepsilon}$ is the strain rate. E is the dynamic Young's modulus of the specimen material, Y is the yield strength under the quasi-static conditions, $\dot{\varepsilon}_0$ is the reference strain rate, m and n are the rate sensitivity and the strain hardening exponents, respectively, α is a fitting parameter, and Y_d is the dynamic yield stress given by

$$Y_d = Y + \alpha\left(\frac{\dot{\varepsilon}}{\dot{\varepsilon}_0}\right)^m. \quad (4)$$

The first and second terms of the second equation in Eq. (3) describe the strain hardening effect and the strain rate effect on the stress.

The dynamic Young's modulus can be expressed as $E = \frac{Y_d}{\varepsilon_y}$. Thus, Eq. (3) may equally be written as

$$\sigma = \begin{cases} \left(Y + \alpha\left(\frac{\dot{\varepsilon}}{\dot{\varepsilon}_0}\right)^m\right)\frac{\varepsilon}{\varepsilon_y}, & \varepsilon \leq \varepsilon_y, \\ Y\left(\frac{\varepsilon}{\varepsilon_y}\right)^n + \alpha\left(\frac{\dot{\varepsilon}}{\dot{\varepsilon}_0}\right)^m, & \varepsilon_y < \varepsilon < \varepsilon_d, \end{cases} \quad (5)$$

where ε_y and ε_d are the yield strain and the densification strain for the frozen soil. In all the conducted tests, ε_d cannot be achieved because of the relatively low stress level.

Due to the thermal sensitivity of the frozen soil, a term that describes the temperature effect is introduced as

$$T^* = \left(\frac{T - T_r}{T_m - T_r} \right)^l, \quad (6)$$

where T is the temperature of the material, T_r is the room temperature, 293 K, T_m is the melting point of the frozen soil, which here is set as 273 K, and l is the thermal exponent.

Then, Eq. (3) can be modified to

$$\sigma = \begin{cases} \left(Y + \alpha \left(\frac{\dot{\varepsilon}}{\dot{\varepsilon}_0} \right)^m \right) \frac{\varepsilon}{\varepsilon_y} T^*, & \varepsilon \leq \varepsilon_y, \\ \left(Y \left(\frac{\varepsilon}{\varepsilon_y} \right)^n + \alpha \left(\frac{\dot{\varepsilon}}{\dot{\varepsilon}_0} \right)^m \right) T^*, & \varepsilon_y < \varepsilon < \varepsilon_d. \end{cases} \quad (7)$$

Set the yield strain to be the strain corresponding to the yield strength. From Fig. 8, it seems that the yield strains of all the confined stress-strain profiles for the frozen soil are insensitive to the strain rate and the temperature. Thus, we set it as 0.015, and the reference strain rate $\dot{\varepsilon}_0$ is 900 s^{-1} . The other material constants are obtained by curve fitting.

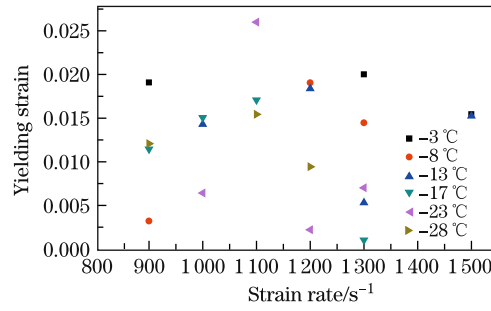


Fig. 8 Yield strain vs. strain rate data

The values of all the material constants are shown in Table 2.

Table 2 Material constants in model

Y/MPa	α/MPa	l	m	n	$\dot{\varepsilon}_0/\text{s}^{-1}$	T_r/K	T_m/K
6	4	1.2	0.287	0.5	900	293	273

Figure 9 compares the dynamic stress-strain curves for the frozen soil under the nearly uniaxially strained conditions from the test and model simulations of -17°C at 1100 s^{-1} and -23°C at 1300 s^{-1} . The predicted tendencies of the model correspond well with the test results in general. However, the results of the tests are scattered so much because of the heterogeneity of the frozen soil. Thus, an accurate fit to the model cannot be accomplished.

6 Conclusions

The dynamic response of the frozen soil is investigated with the SHPB under the uniaxial stress and nearly uniaxial strain conditions. The frozen soil exhibits the sensitivity to the strain rate and the temperature at both of the two conditions. With the confinement, the frozen soil shows an elastic-plastic behavior. The lateral confinement restricts the evolution of the damage in the samples and the radial deformation of the frozen soil, inducing the compaction and the higher capability. The specimens under the uniaxial stress conditions break up into several pieces after the test. A phenomenological model is constructed to describe the temperature

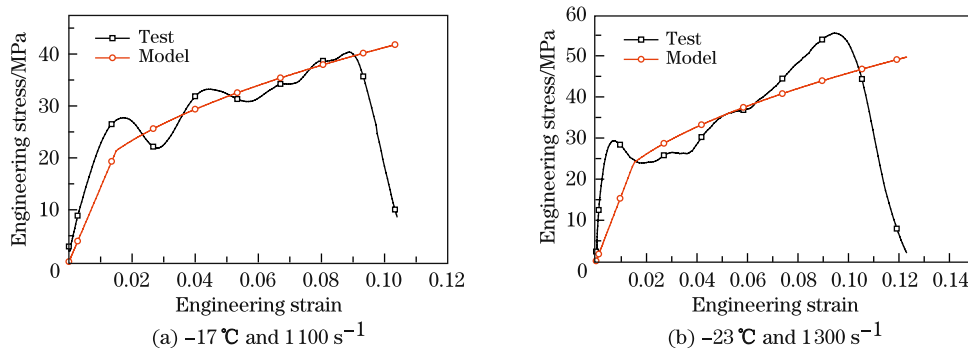


Fig. 9 Comparison of dynamic stress-strain curves for confined frozen soil

and the strain-rate-dependent stress-strain behavior of the frozen soil. This model is capable of expressing such tendencies and yet simple enough for the FEM simulations. However, this model cannot describe the behavior of the frozen soil in the three-dimensional situations at present. Therefore, improving this model to general conditions will be the further work.

References

- [1] Xu, X. Z., Wang, C. J., and Zhang, L. X. *Physics of Frozen Soil* (in Chinese), Science Press, Beijing (1997)
- [2] Zhao, S. P., Zhu, Y. L., He, P., and Yang, C. S. Recent progress and suggestion in the research on dynamic response of frozen soil (in Chinese). *Journal of Glaciology and Geocryology*, **24**(5), 681–686 (2002)
- [3] Ma, Q. Y. Research status of dynamic properties of artificial frozen soil and its significance (in Chinese). *Rock and Soil Mechanics*, **30**(supp.), 10–14 (2009)
- [4] Martin, B. E., Chen, W., and Song, B. Moisture effects on the high strain-rate behavior of sand. *Mechanics of Materials*, **41**(6), 786–798 (2009)
- [5] Song, B., Chen, W. N., and Luk, V. Impact compressive response of dry sand. *Mechanics of Materials*, **41**(6), 777–785 (2009)
- [6] Furish, M. D. *Measuring Static and Dynamic Properties of Frozen Silty Soils*, Sandia Report, 98-1479, Livermore, California, U.S.A. (1998)
- [7] Lee, M. Y., Fossum, A., and Costin, L. S. *Frozen Soil Material Testing and Constitutive Modeling*, Sandia Report, 2002-0524, Livermore, California, U.S.A. (2002)
- [8] Ma, Q. Y. Experimental analysis of dynamic mechanical properties for artificially frozen clay by the split Hopkinson pressure bar. *Journal of Applied Mechanics and Technical Physics*, **51**(3), 448–452 (2010)
- [9] Kolsky, H. An investigation of the mechanical properties of materials at very high rates of loading. *Proc. Phys. Soc. B*, **62**(11), 676–700 (1949)
- [10] Gao, W. J., Shan, R. L., Wang, G. C., and Cheng, R. Q. Constitutive relation of Yunjialing anthracite under medium strain rate. *Journal of China University of Mining & Technology*, **17**(1), 126–132 (2007)
- [11] Zhu, Z. W., Ning, J. G., and Liu, X. Dynamic mechanical behavior of soil under impact load (in Chinese), *Chinese Journal of High Pressure Physics*, **25**(5), 444–450 (2011)
- [12] Shazly, M., Prakash, V., and Lerch, B. A. Confinement effects on the dynamic compressive properties of an epoxy syntactic foam. *International Journal of Solids and Structures*, **46**(6), 1499–1515 (2007)
- [13] Song, B., Chen, W. N., Yanagita, T., and Frew, D. J. Confinement effects on the dynamic compressive properties of an epoxy syntactic foam. *Composite Structures*, **67**(3), 279–287 (2005)
- [14] Warren, T. L. and Forrestal, M. J. Effects of strain hardening and strain-rate sensitivity on the penetration of aluminum targets with spherical-nosed rods. *International Journal of Solids and Structures*, **35**(28-29), 3737–3753 (1998)